7

Efficient Simulation of Transient Heat Transfer Problems in Civil Engineering

Sebastian Bindick, Benjamin Ahrenholz, Manfred Krafczyk
Institute for Computational Modeling in Civil Engineering, Technische Universitet Braunschweig
Germany

1. Introduction

Heat transport problems arise in many fields of civil engineering e.g. indoor climate comfort, building insulation, HVAC (heating, ventilating, and air conditioning) or fire prevention to name a few. An a priori and precise knowledge of the thermal behavior is indispensable for an efficient optimization and planning process. The complex space-time behavior of heat transfer in 3D domains can only be achieved with extensive computer simulations (or prohibitively complex experiments). In this article we describe approaches to simulate the transient coupled modes of heat transfer (convection, conduction and radiation) applicable to many fields in civil engineering. The numerical simulation of these coupled multi-scale, multi-physics problems are still very challenging and require great care in modeling the different spatio-temporal scales of the problem. One approach in this direction is offered by the Lattice-Boltzmann method (LBM) which is known to be a viable Ansatz for simulating physically complex problems. For the simulation of radiation a radiosity method is used which also has already proven its suitability for modeling radiation based heat transfer. The coupling and some typical applications of both methods are discussed in this chapter.

2. Modeling thermal flows with Lattice-Boltzmann

In the last two decades the Lattice-Boltzmann-Methods (LBM) has matured as an efficient alternative to discretizing macroscopic transport equations such as the Navier-Stokes equations describing coupled transport problems such as thermal flows. The Boltzmann equation describes the dynamics of a propability distribution function of particles with a microscopic particle velocity under the influence of a collision operator. Macroscopic quantities such as the fields of density, flow velocities, energy or heat fluxes are consistently computed as moments of ascending order from the solution. For flow problems the Boltzmann equation can be drastically simplified by discretizing the microscopic velocity space and by using a simplified collision operator. A non-trivial yet algorithmically straight forward Finite Difference discretization for this set of PDEs results in the Lattice-Boltzmann equations. For the simulation of thermal driven flows using the LB method a hybrid thermal LB model (Hybrid TLBE) has been established, i.e. an explicit coupling between an athermal LBE scheme for the flow part and a separate Lattice-Boltzmann equation for the temperature equation.

2.1 An overview of the physical background of lattice Boltzmann models

The origin of the physical modeling process is the fact that the physical scope of validity of the Boltzmann equation includes the Navier-Stokes equations as well. In the framework of the kinetic gas theory it can be shown that the Navier-Stokes equations can be derived from the Boltzmann equation in the limit of small Knudsen numbers if the hydrodynamic momentum and pressure fields are described as low order moments of the primary variables of the Boltzmann equation (i.e. probability distributions). This implies that approximate solutions of the Boltzmann equations and their resulting moments can be used to calculate approximate solutions for the corresponding Navier-Stokes equations (Succi, 2001; He & Luo, 1997b; Bhatnagar et al., 1954). A direct discretization of the full Boltzmann equation is neither useful nor necessary for most macroscopic flow problems; therefore, the following simplifications are typically made: First, the collision operator in the so-called BGK or Multiple-Relaxation-Time (MRT) approximation is considered, which assumes that the particle system is statistically close to a kinetic equilibrium. Furthermore, the microscopic velocity space is discretized to develop a system of discrete Boltzmann equations, instead of the Boltzmann equation in BGK-approximation. These discrete equations contain a constant prefactor in the convective term, which suggests a discretization along the corresponding characteristics. This system of discrete Boltzmann equations can be numerically discretized in different ways. The model relationships are outlined in Figure 1.

Historically, LBM originated from the lattice gas automata [LGA], which can be considered as a simplified, fictitious molecular dynamics in which space, time, and particle velocities are all discrete. However, it was discovered that LGA suffers from several inherent defects including

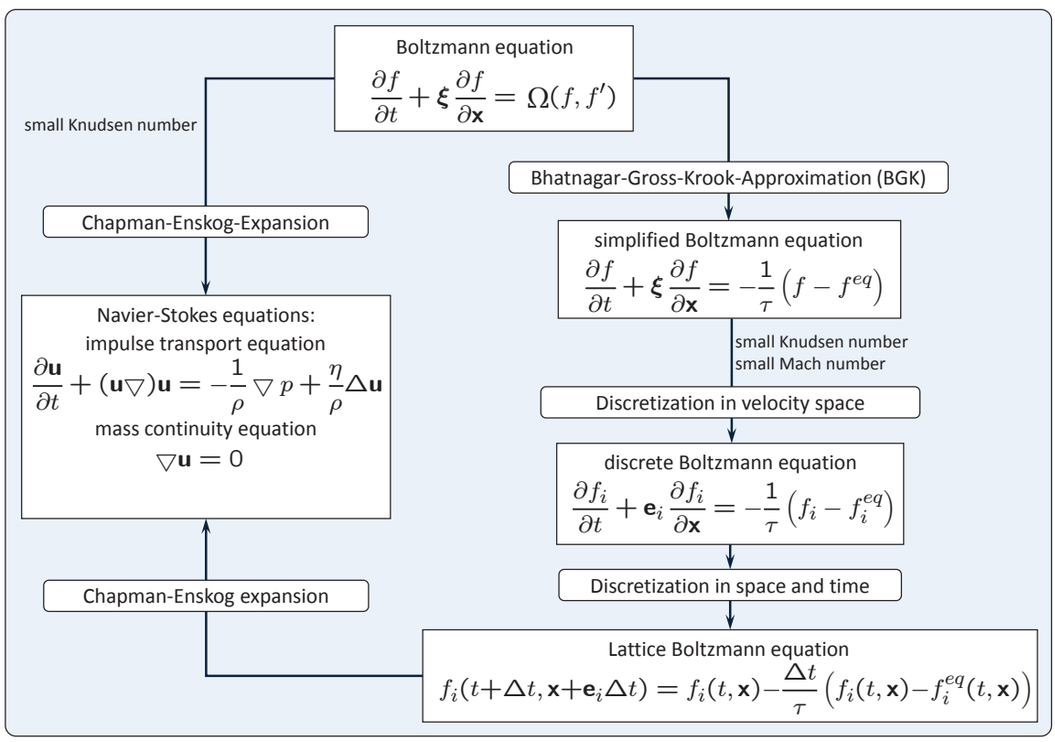

Fig. 1. From the Boltzmann equation to Navier-Stokes

the lack of Galilean invariance (except for $\rho = constant$), the presence of statistical noise and the absence of exponential complexity for three-dimensional lattices. The main motivation for the transition from LGA to LBM was the desire to remove statistical noise by replacing the Boolean particle number in a lattice direction with its ensemble average, the so-called density distribution function. Accompanying this replacement, the discrete collision rules also have to be modified as a continuous function - the collision operator. The first LBM has been proposed by (McNamara & Zanetti, 1988) and improved by (Higuera & Jiménez, 1989; Higuera et al., 1989). However, the connection to the Boltzmann equation (introduced by the Austrian physicist Ludwig Boltzmann in 1872) has been proven afterwards (He & Luo, 1997b; Sterling & Chen, 1996). The Boltzmann equation describes the statistical distribution of one particle in a fluid and the probability to encounter this particle at time t with velocity $\boldsymbol{\xi}$ at location x (Cercignani et al., 1994; Cercignani & Penrose, 1998):

$$\frac{\partial f}{\partial t} + \boldsymbol{\xi} \cdot \frac{\partial f}{\partial \mathsf{x}} + \mathsf{F} \cdot \frac{\partial f}{\partial \boldsymbol{\xi}} = \Omega(f, f') \tag{1}$$

In the LBM development, an important simplification is the approximation of the collision operator with the Bhatnagar-Gross-Krook (BGK) relaxation term. This lattice BGK (LBGK) model renders simulations more efficient and allows flexibility of the transport coefficients. On the other hand, it has been shown that the LBM scheme can also be considered as a special discretized form of the continuous Boltzmann equation. Through a Chapman-Enskog expansion (Frisch et al., 1987; Qian et al., 1992) or an asymptotic analysis (Junk et al., 2005), one can recover the governing continuity and Navier-Stokes equations (Equation 2) from the LBM algorithm (Qian et al., 1992).

$$\frac{\partial \mathsf{u}}{\partial t} + (\mathsf{u}\nabla)\mathsf{u} = -\frac{1}{\rho}\nabla p + \frac{\mu}{\rho}\Delta \mathsf{u}, \tag{2a}$$

$$\nabla \mathsf{u} = 0 \tag{2b}$$

In addition, the pressure field is also directly available from the density distributions as $p = c_S^2\ \rho$ where c_s is the speed of sound and hence there is no additional Poisson equation to be solved as in traditional CFD methods.

A particularly effective form of discretization is obtained if the spatial grid is being chosen so that the advection of the distribution functions follows exactly the characteristics defined by the microscopic particle velocities, i.e. if the physical discretization of the microscopic velocity space (after multiplying it with the appropriate local time step) is congruent with the numerical grid. This leads to a relatively simple Finite-difference approach. With the help of an appropriate multi-scale expansion it can be shown that the moments of zero to second order are approximate solutions of the velocity and pressure tensor of the Navier-Stokes equations, given that the relaxation time included in the BGK-operator is defined as a linear function of the kinematic viscosity. Yet, this scheme would not be competitive without further modifications. Theoretical analysis allows to determine a global constant numerical viscosity, which can be eliminated by appropriate scaling, resulting in a method of quadratic accuracy in space for the Navier-Stokes equations. A detailed description of the underlying derivations can be found in (Qian et al., 1992; Chen & Doolen, 1998; Succi, 2001; Dellar, 2003; He & Luo, 1997a;b; Bhatnagar et al., 1954) The accuracy of the method in the fluid depends, like for all transport problems mainly on the quality of the boundary conditions. In contrast to the direct discretization of the Navier-Stokes equations corresponding initial- and boundary conditions must be specified for the probability distributions within LBM.

Different approaches have been developed regarding accuracy and consistency and have been analyzed in the corresponding literature see e.g. (Junk et al., 2005; Ginzburg & d'Humières, 1996; d'Humières et al., 2002). Since typical LBM discretizations are based on Cartesian grids, it represents a curved surface only with first order accuracy. For second order accurate fluid/wall boundary conditions it is necessary to compute the projection of the node links to the surface of the geometry and incorporate them into the discretization scheme for the boundary conditions. If MRT approaches (d'Humières et al., 2002) are used, boundary conditions for pressure and velocities can be enforced with second order accuracy. The application of hierarchical Cartesian grid allows the use of tree type data structures and enables a hierarchical time-step procedure with an optimal Courant number of one at each grid level, i.e. on coarse grid cells only a correspondingly coarser time step is necessary (Tlke et al., 2006). The issue of efficiency of the LB method in direct comparison with state-of-the-art FE and FV-discretizations of the Navier-Stokes equations is discussed e.g. in (Geller et al., 2006).

Unlike the traditional computational fluid dynamics (CFD), which numerically solves the conservation equations of macroscopic properties (i. e., mass, momentum, and energy), LBM models the fluid consisting of fictitious particles, which perform consecutive propagation and collision processes over a discrete lattice. Due to its particulate nature and local dynamics, LBM is very efficient when dealing with complex boundaries and the incorporation of microscopic interactions.

2.2 A short introduction to the lattice Boltzmann method

The LB method is a numerical method to solve the Navier-Stokes equations Frisch et al. (1987); Benzi et al. (1992); Chen & Doolen (1998), where density distributions propagate and collide on a regular lattice. A common labeling for different lattice Boltzmann models is DdQq (Qian et al., 1992), where d is the space dimension and q the number of microscopic velocities. Besides the most common D3Q19 models (Figure 2) one can often find D3Q15 stencils (Figure 2) in 3D and D2Q9 in 2D (Figure 3) as well as non local stencils like D3Q27 or D3Q39. D3Q13 uses a reduced set of velocities, however it is very promising due to an excellent ratio between accuracy and computational requirements (d'Humières et al., 2001; Tlke & Krafczyk, 2008).

In the following section x represents a 3D vector in space and $\boldsymbol{f}$ a b-dimensional vector, where

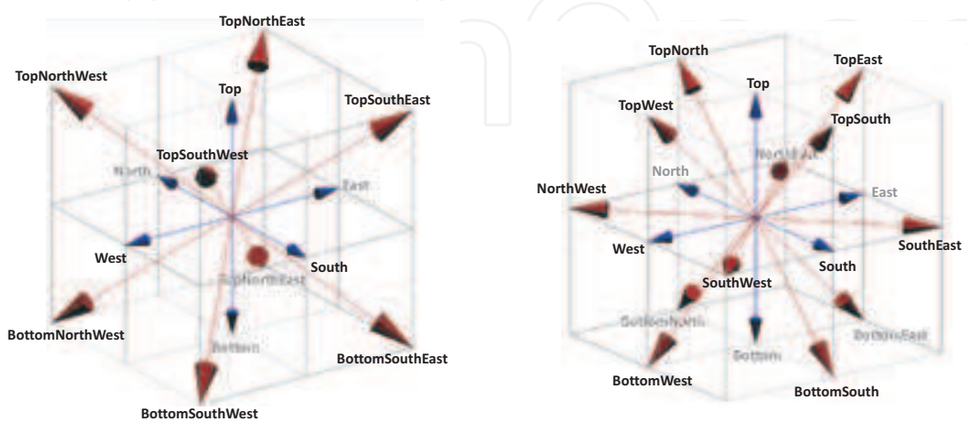

Fig. 2. D3Q19- and D3Q15 stencils, the most common representatives in 3D

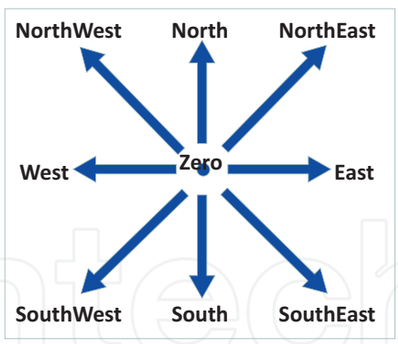

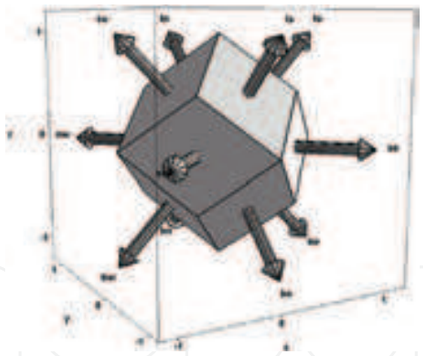

Fig. 3. D2Q9 stencil commonly used for 2D LBM and D3Q13 - the smallest stencil for a space filling grid in 3D

b is the number of microscopic velocities. The 19 velocities are given as

$$\mathsf{e}_i, i = 0,\ldots,18\} = \begin{pmatrix} 0 & c & -c & 0 & 0 & 0 & 0 & c & -c & c & -c & c & -c & c & -c & 0 & 0 & 0 & 0 \\ 0 & 0 & 0 & c & -c & 0 & 0 & c & -c & -c & c & 0 & 0 & 0 & 0 & c & -c & c & -c \\ 0 & 0 & 0 & 0 & 0 & c & -c & 0 & 0 & 0 & 0 & c & -c & -c & c & c & -c & -c & c \end{pmatrix}$$

where c is a constant microscopic reference velocity related to the speed of sound by $c_s^2 = c^2/3$. The microscopic velocities define a space-filling computational lattice where a node is connected to the neighboring nodes through the vectors $\{\Delta t\, \mathsf{e}_i, i = 0,\ldots,18\}$. The generalized lattice Boltzmann equation (GLBE) using the Multiple-Relaxation-Time model introduced by (d'Humières, 1992; Lallemand & Luo, 2000) is given by

$$f_i(t + \Delta t, \mathsf{x} + \mathsf{e}_i \Delta t) = f_i(t, \mathsf{x}) + \Omega_i, \quad i = 0,\ldots,b-1, \tag{3}$$

where f_i are mass fractions (unit kg m^{-3}) propagating with velocities e_i, Δt is the time step, the grid spacing is $\Delta x = c\Delta t$, and the collision operator of the Multiple-Relaxation-Time model (MRT) is given by

$$\Omega = \mathsf{M}^{-1}\mathsf{S}\left((\mathsf{M}\boldsymbol{f}) - \boldsymbol{m}^{eq}\right). \tag{4}$$

The matrix M is used to transform the distributions into moment space. The resulting moments $\boldsymbol{m} = \mathsf{M}\boldsymbol{f}$ are labeled as

$$\boldsymbol{m} = (\delta\rho, e, \epsilon, j_x, q_x, j_y, q_y, j_z, q_z, 3p_{xx}, 3\pi_{xx}, p_{ww}, \pi_{ww}, p_{xy}, p_{yz}, p_{xz}, m_x, m_y, m_z),$$

where $\delta\rho$ is a density variation related to the pressure variation δp by

$$\delta p = \frac{c^2}{3}\delta\rho. \tag{5}$$

and where $(j_x, j_y, j_z) = \rho_0(u_x, u_y, u_z)$ is the momentum and ρ_0 is a constant reference density. The moments $e, p_{xx}, p_{ww}, p_{xy}, p_{yz}, p_{xz}$ of second order are related to the stress tensor (Equation 6). The other moments of higher order are related to higher order derivatives of the flow field and have no direct physical impact with respect to the incompressible Navier-Stokes equations.

$$\sigma_{\alpha\beta} = -p\delta_{\alpha\beta} + \rho\nu(\frac{\partial u_\alpha}{\partial x_\beta} + \frac{\partial u_\beta}{\partial x_\alpha}) \tag{6}$$

The matrix S is a diagonal collision matrix composed of relaxation rates $\{s_{i,i}, \ldots, b-1\}$, also called the eigenvalues of the collision matrix $\mathsf{M}^{-1}\,\mathsf{S}\,\mathsf{M}$. The rates different from zero are

$$\begin{aligned} s_{1,1} &= -s_e \\ s_{2,2} &= -s_\epsilon \\ s_{4,4} = s_{6,6} &= s_{8,8} = -s_q \\ s_{10,10} = s_{12,12} &= -s_\pi \\ s_{9,9} = s_{11,11} = s_{13,13} &= s_{14,14} = s_{15,15} = -s_\nu \\ s_{16,16} = s_{17,17} &= s_{18,18} = -s_m. \end{aligned}$$

The relaxation rate s_ν is related to the kinematic viscosity ν by

$$s_\nu = \frac{1}{3\frac{\nu}{c^2\Delta t} + \frac{1}{2}}. \tag{7}$$

The remaining relaxation rates $s_e, s_\epsilon, s_q, s_\pi$ and s_m can be freely chosen in the range of $[0,2]$ and may be tuned to improve accuracy as well as stability (Lallemand & Luo, 2000) of the model. The optimum values depend on the specific system under consideration (geometry, initial, and boundary conditions) and can therefore not be computed in advance for general cases.
In summary it may be noted that if one uses either a Chapman-Enskog expansion (Frisch et al., 1987) or an asymptotic expansion using the diffusive scaling (Junk et al., 2005), it can be shown that the lattice Boltzmann method is a scheme of first order in time and second order in space for the incompressible Navier-Stokes equations.

2.3 Thermal flows

During the last decade different approaches for the simulation of thermal driven flows using the LB method have been developed (Alexander et al., 1993; Vahala et al., 2000; Shan, 1997; Qian, 1993; Filippova & Hänel, 2000; Lallemand & Luo, 2003). Energy conserving thermal LB equation models (TLBE) use a larger set of discrete velocities than the standard method (Qian et al., 1992) to include a thermal variable, such as temperature. The internal energy is defined by a second-order moment of the distribution function, and the collision operator is chosen to satisfy local energy conservation. However, these thermal flow simulations utilizing the thermal lattice Boltzmann equation (TLBE) are hampered by numerical instabilities caused by an algebraic coupling among different modes of the linearized collision operator, independently of the number of discrete velocities used in the model (Lallemand & Luo, 2003). To avoid the limitations of TLBE a hybrid scheme was developed in (Lallemand & Luo, 2003) by coupling the energy mode of the athermal LB model to the temperature field. This method has been extended for turbulent flows by (van Treeck et al., 2006) and is usually referred to as hybrid thermal lattice Boltzmann equation (HTLBE).
In this work the temperature equation is discretized by the following finite difference (FD) scheme:

$$\frac{T_{i,j,k}(t+\Delta t^{FD}) - T_{i,j,k}(t)}{\Delta t^{FD}} = -\vec{j}_{i,j,k}(t)\nabla^{(h)}_{i,j,k} T_{i,j,k}(t) + \alpha \triangle^{(h)}_{i,j,k} T_{i,j,k}(t) \tag{8}$$

where α is the thermal diffusivity. For computing the difference operators $\nabla^{(h)}_{i,j,k}$ and $\triangle^{(h)}_{i,j,k}$ a 6 point stencil is used. The coupling of both schemes is explicit, meaning that the velocity field obtained by the MRT scheme is inserted into the energy equation while the solution of the latter is used to compute the buoyant force $F_z(\vec{x},t)$ in the sense of a Boussinesq approximation. For a given Rayleigh number

$$Ra = \frac{Prg_z\beta\Delta TL^3}{\nu^2} \tag{9}$$

and Prandtl number $Pr = \nu/\alpha$ and by setting $\beta = 1/T_0$, the parameters viscosity ν and diffusivity α are obtained and the relaxation coefficients can be determined with the formulae given in (Lallemand & Luo, 2003), while ν has to fulfill the stability constraints of the MRT scheme. L is a characteristic length scale of the dimensionless system, i.e. given in lattice units. The coupling of the temperature field to the energy mode of the LB model is done by inserting the temperature into the equilibrium moments (Tlke, 2006):

$$m_1^{eq} = ((3T-1) + (u_x^2 + u_y^2 + u_z^2))\rho_0 \tag{10}$$

$$m_2^{eq} = (1 - 1.8T)\rho_0 \tag{11}$$

where $T = T(t,i,j,k)$ is a dimensionless temperature varying in space and time.
In order to simulate more realistic engineering applications, such as convective heat transport in buildings, simulations with Reynolds numbers of more than 10^6 have to be performed. At this scale DNS simulations become too expensive and therefore it is necessary to extend the standard HTLBE by a turbulence model. Large-eddy (LES) approaches are regarded as a promising compromise between explicit modeling of all scales of the turbulent spectrum and direct numerical simulation (DNS). In LES the large scale motions of the flow are calculated, while the effect of the smaller universal scales (the so called sub-grid scales) are modeled using a sub-grid scale (SGS) model. The most commonly used SGS model is the Smagorinsky model. It compensates for the unresolved turbulent scales through the addition of a so-called eddy viscosity into the governing equations.
In the context of lattice Boltzmann, the LES approach has first been used by (Hou et al., 1994) in 2D and in (Krafczyk et al., 2003) in 3D. As an inherent property of the LBE scheme, components of the momentum flux tensor, here expressed in terms of moments,

$$\Pi_{\alpha\beta} = \sum_i e_{i\alpha}e_{i\beta}f_i \tag{12}$$

are given as local quantities and do not have to be computed from derivatives of hydrodynamic quantities. Therefore, the local strain tensor is obtained by the relation

$$\tilde{\epsilon}_{\alpha\beta} = \frac{s_{xx}}{2\rho C_s^2}(C_s^2\rho\delta_{\alpha\beta} + \rho u_\alpha u_\beta - \Pi_{\alpha\beta}) \tag{13}$$

as previously shown by (Krafczyk et al., 2003). Consequently, the molecular and turbulent viscosities can be added to form a total viscosity $\nu_{total} = \nu_0 + \nu_T$ which substitutes the material property by a space and time-dependent quantity. Having computed a local value for ν_T, the relaxation parameter s'_{xx} for the second order moments related to the stress tensor components $p_{xx}, p_{ww}, p_{xy}, p_{yz}$ and p_{zx} can be determined by

$$s'_{xx} = \frac{1}{3(\nu_0 + \nu_T) + \frac{1}{2}} \quad , \tag{14}$$

where ν_T is either related to the same time step or the last time step before propagation of the explicit scheme. Due to consistency reasons a subgrid model is also used for heat flux as proposed in (van Treeck et al., 2006).

3. Radiative heat transfer using the Radiosity-method

In this section an approach for radiative heat transfer in 3d domains based on the hierarchical radiosity method coupled to the LB method is presented. The radiosity method assumes radiative exchange between gray, diffuse surfaces in a radiatively non-participating medium. The idea is to hierarchically subdivide surfaces forming a quad-tree structure until a refinement criterion is reached. The fundamental underlying operation of the radiosity method is visibility detection which can be solved efficiently by using a space partitioning approach for the input surfaces. For this reason a kd-tree is chosen which is the most efficient method for visibility detection on irregularly distributed surfaces. These approaches dramatically decrease the complexity of the radiation problem from $O(n^3)$ to $O((k^2+n)\log k)$, where k is the number of input surfaces and n is the number of refined surfaces. For validations of these approach for several non-trivial examples, demonstrating that this scheme is second-order accurate see (Bindick et al., 2010).

3.1 Modeling radiative heat transfer

Heat flux from a body induced by thermal radiation solely depends on the local surface temperature and is not bound to molecular transport. This implies that every body is not only interacting with its direct neighbors but with all visible elements. Thermal radiation incident to a surface may be partially absorbed, reflected or transmitted. Here the absorbed part will be transformed into thermal energy. The complex radiative processes at a solid body are depicted in Fig.4.

The energy flux $M(\lambda, T)$ emitted from a surface with the temperature T and the wavelength λ can be described through the Planck's law of black-body radiation:

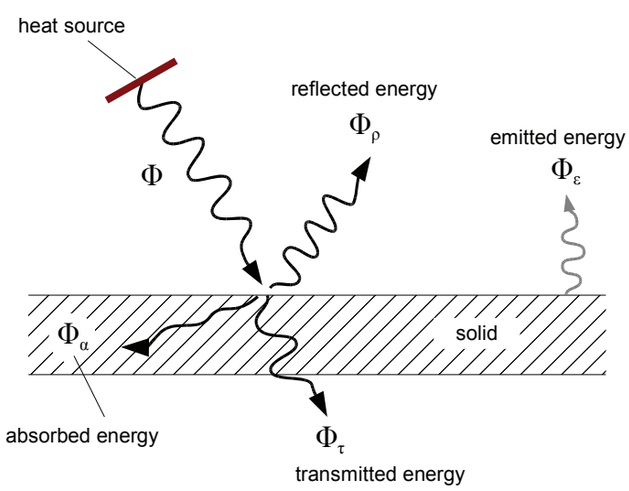

Fig. 4. Radiative processes at a solid body

$$M(\lambda, T) = \frac{2\pi c_0^2}{h^4} \frac{A}{e^{(hc_0/k\lambda T)} - 1} d\lambda \quad [W], \tag{15}$$

with the Planck constant $h = 6,626 \cdot 10^{-34}\ J \cdot s$, the speed of light c_0 and the Boltzmann constant $k = 1,381 \cdot 10^{-23}\ J/K$. This energy distribution is not constant over the spectrum and rises with increasing wavelength until a maximum at λ_{max} is reached (Siegel & Howell, 2002).
The energy flux leaving or entering a body depending on the direction in space can be described by the irradiance (E), the radiant energy arriving at a surface:

$$E = \int_\Omega I_a \cos(\Theta)\ d\Omega \quad \left[\frac{W}{m^2}\right] \tag{16}$$

with the radiative intensity I_a depending on the wavelength and $\cos(\Theta)\ d\Omega$ representing the projection of the solid angle. Analogously, the radiosity B (the radiant energy leaving a surface) can be written as:

$$B = \int_\Omega I_l \cos(\Theta)\ d\Omega \quad \left[\frac{W}{m^2}\right]. \tag{17}$$

In the following sections we describe how to solve the corresponding equations for a full radiant energy exchange in an enclosed 3d domain using the radiosity method (Goral et al., 1984).
The fundamentals of radiative heat transfer are explained in detail in e.g. (Siegel & Howell, 2002), (Modest, 2003), (Baehr & Stephan, 2006) and (Welty et al., 2001).

3.2 The classical radiosity method

The full energy exchange between diffuse surfaces can be calculated by forming an energy equilibrium for Eq. (16) and Eq. (17) in an enclosed environment. This approach leads to the radiosity method (based on the zonal method (Hottel & Cohen, 1958)) often used in the field of computer graphics to compute the inter-reflections of light (global illumination) (Goral et al., 1984). The radiosity method has long been an active field of research and many improvements could be found to reduce the algorithmic complexity of the problem. The radiosity method comes with the assumption that all bodies are gray diffusive reflectors, emitters and absorbers, (i.e. the same amount of radiant energy is reflected, emitted and absorbed in all directions) which is a common approximations for real bodies. Another assumption is that the radiative heat transfer between surfaces is separated by vacuum (radiatively nonparticipating), without considering the absorbing, scattering and emitting effects of the medium. This is a common approach for the relatively low pressures and temperatures that occur in many engineering applications. By subdividing the geometry surfaces into small planar patches, with homogeneous material properties, the discrete radiosity equation can be written as the sum of the patch radiation E_i and the radiosity B_j of all other n patches multiplied with the diffuse reflectivity ρ_d:

$$B_i = E_i + \rho_d \sum_{j=1}^{n} B_j F_{ij}, \tag{18}$$

with the configuration factor F_{ij} depending on the geometrical relation between two patches (see Fig.5).

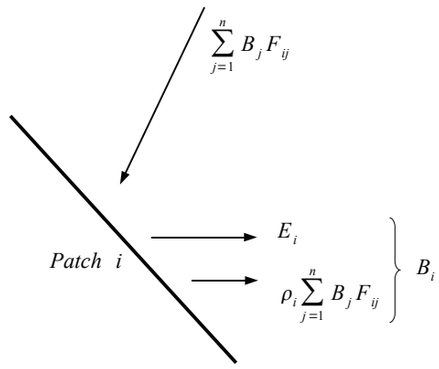

Fig. 5. Radiosity method

The configuration factor F_{ij} (also known as form factor or view factor) appearing in Eq. (18) describes the fraction of diffuse energy leaving a surface and directly reaching another surface (Goral et al., 1984). The configuration factor can be calculated by the following double integral which describes the relative position and orientation between two patches p_i and p_j:

$$F_{ij} = \frac{1}{A_i} \int_{A_i} \int_{A_j} \frac{\cos(\Theta_i)\cos(\Theta_j)}{\pi r^2} \, V(p_i, p_j) \, dA_i \, dA_j, \tag{19}$$

with the approximation of the solid angle $\frac{\cos(\Theta_i)\cos(\Theta_j)}{\pi r^2}$, the area A_i and A_j of surface i and j and a binary visibility function $V(p_i, p_j)$ to describe the visibility between two surfaces:

$$V(p_i, p_j) \quad \begin{cases} 1 \text{ if } p_i \text{ and } p_j \text{ are visible to each other} \\ 0 \text{ else} \end{cases}. \tag{20}$$

An analytic solution for Eq. 19 can only be found for very simple geometric configurations. A catalog of 300 known radiation configuration factors was published by Howell (Howell, 1982). The configuration factors for complex 3d geometries can not be determined analytically and in general have to be computed numerically as described below.
The kernel of Eq. (19), which is called differential form of the configuration factor, corresponds to the differential area of two patches, illustrated in Figure 6:

$$F_{ij} = \frac{\cos(\Theta_i)\cos(\Theta_j)}{\pi r^2} \, dA_j. \tag{21}$$

This expression represents the simplest approximation of the configuration factor and is only applicable for small patches with large distances to other patches and causes singularity problems.
Finding a general and accurate solution for the configuration factor F_{ij} has long been an active field of research (Tampieri, 1992; Cohen & Greenberg, 1985; Pianykh et al., 1998; Siegel & Howell, 2002). For this reason several numerical approaches to approximately solve the configuration factor integral exist. Early methods used a hemicube (Cohen & Greenberg, 1985) which comes with high memory requirements and makes it unusable for simulations with complex geometry models. A better approach combines adaptive mesh refinement (explained in detail in the following Sec. 3.3) with a point-to-disk approximation of the configuration factor (Wallace et al., 1989; Pianykh et al., 1998; Pellegrini, 1995; Siegel & Howell, 2002). Considering the configuration factor between a differential area and an arbitrarily oriented

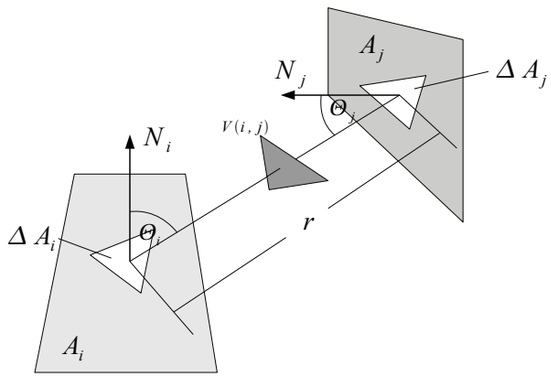

Fig. 6. Notation for configuration factor

disk Eq. (19) changes to:

$$F_{ij} = V(p_i, p_j) \frac{\cos(\Theta_i)\cos(\Theta_j)A_j}{\pi r^2 + A_i}, \tag{22}$$

where r is the distance between the patches. This approach was first introduced by Wallace (Wallace et al., 1989) and has been established as a practical approximation technique to solve the form factor double integral. Here we use the ray tracing algorithm to compute the visibility between two surfaces $V(p_i, p_j)$ where a ray is shot from the center point of the emitter to the center point of the receiver. Each ray must be tested for intersections with all objects in the environment. The ray tracing process can be accelerated substantially by using optimized hierarchical data structures based on kd-trees (see Sec. 3.4), so that logarithmic complexity as a function of the number of scene primitives can be achieved.
For a full radiative exchange in a closed environment Eq. (18) has to be solved simultaneously for all patches. These n equations form the following system of linear equations:

$$\begin{pmatrix} 1-\rho_1 F_{11} & -\rho_1 F_{12} & ... & -\rho_1 F_{1n} \\ -\rho_2 F_{21} & 1-\rho_2 F_{22} & ... & -\rho_2 F_{2n} \\ ... & ... & ... & ... \\ -\rho_n F_{n1} & -\rho_n F_{n2} & ... & 1-\rho_n F_{nn} \end{pmatrix} \begin{pmatrix} B_1 \\ B_2 \\ ... \\ B_n \end{pmatrix} = \begin{pmatrix} E_1 \\ E_2 \\ ... \\ E_n \end{pmatrix} \tag{23}$$

Solving this equation system yields the average radiosity value for each patch. Here an efficient solution technique called progressive refinement has been established, where the energy from a single patch is iteratively shot to the rest of the domain (Cohen et al., 1988). After the first iteration step only the patches in direct line of sight of an emitting patch will be affected. With every further step the indirectly irradiated patches will receive more energy. The shooting method utilizes the diagonal dominance of the interaction matrix and has proven to be an efficient solution technique (Cohen et al., 1988).

3.3 Hierarchical radiosity

The adaptive hierarchical radiosity method reduces the complexity of the standard radiosity method $O(n^2)$ (where all patches are in interaction with each other) to $O(k^2 + n)$ (where k is the number of input (root) patches and n is the number of refined patches) (Hanrahan et al., 1991). The basic idea of this approach is to use fewer and coarser interactions between patches depending on a specified solution accuracy. Receiver and emitter patches are hierarchically subdivided forming a quad-tree structure until a refinement criterion (often called oracle) is

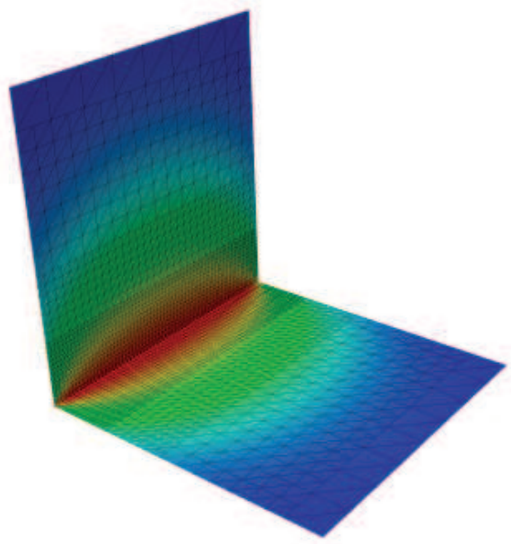

Fig. 7. Adaptive hierarchical subdivision for surfaces with high energy gradients

reached (see Fig.7). The goal is to establish links between patches that can be used for the energy transfer.
The hierarchical radiosity algorithm consists of three steps:

1. Initial linking: The configuration factor (using the disk approximation of Eq. 22) is evaluated for each pair of input patches. If the configuration factor is greater than a specified form factor threshold (F_ε) and a defined area threshold (E_ε) (depending on the required solution accuracy) a recursive subdivision routine is applied for the patch with the larger area. Here the subdivision process increases the accuracy of the solution. Otherwise, if the configuration factor is less than the thresholds a link is created which represents the energy transfer between these two patches. Links can be established between different levels and represent the interactions between groups of patches. This approach decreases the number of patches interacting with each other to $O(k^2 + n)$ where the visibility procedure is defined in section 3.4).
2. Energy gathering: For each patch the energy is repeatedly gathered over the incoming links until a convergence criterion is reached.
3. Push-pull: Energy arriving at a patch has to be propagated through the complete patch hierarchy to reach a consistent state after each iteration step. This can be achieved by pushing down the energy from the upper nodes to the leaf nodes and then pulling the weighted energy of the leafs to the upper ones.

A more detailed description of the hierarchical radiosity method can be found in, e.g. (Shaw, 1997) and (Schäfer, 2000) and for parallel approaches in, e.g. (Bohn & Garmann, 1995), (Podehl et al., 1998) and (Sinop et al., 2005).

3.4 Fast visibility computations based on kd-trees

The ray tracing algorithm is a fundamental operation in the radiosity method for visibility detection between surfaces and is the critical factor to develop a fast radiative heat transport method. Ray tracing can be solved efficiently by using a space partitioning data structure generated in a preprocessing step. Over the past few decades different space subdivision

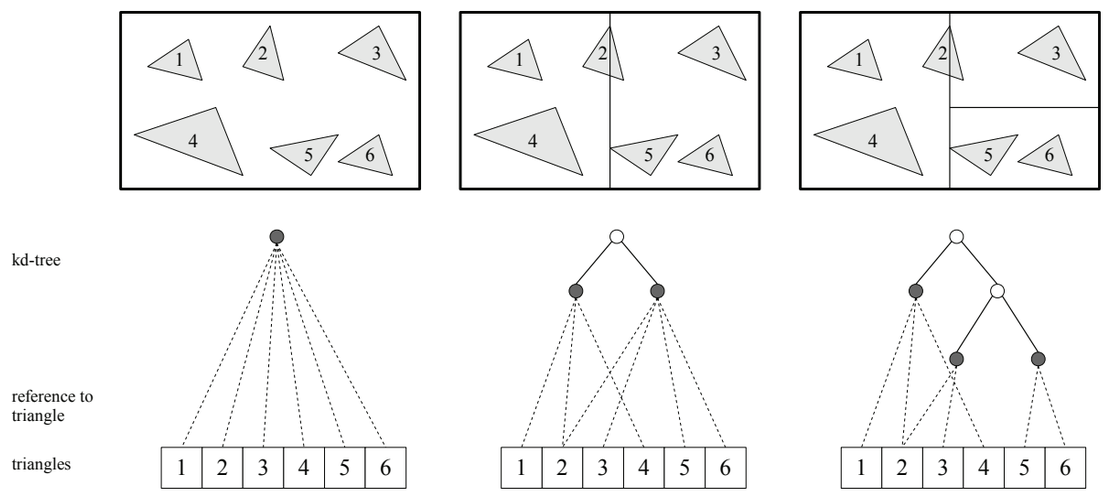

Fig. 8. Kd-tree example in 2D

schemes e.g. regular grids (Fujimoto et al., 1986), octrees (Glassner, 1984) or kd-trees (Havran, 2000) have been examined. Meanwhile kd-trees for ray tracing even for animated scenes have been established as the best known acceleration structure (Havran, 2000; Szirmay-Kalos et al., 2002; Shevtsov et al., 2007).

A kd-tree is a particular form of a Binary Space Partitioning (BSP) tree which always splits the space in axis-aligned cuboids. Each tree node is associated with such a cuboid and stores informations about its physical position in space (center point and length of the edges). The kd-tree root node contains all patches of the scene. The kd-tree is built over the bounding boxes of the surface polygons (mostly triangles or rectangles), often called *patches*). In each recursive construction step, two child nodes of the current node are created. The cuboid associated with the current node is split into two parts, which are then associated with the child nodes, a long with all the patches that overlap them (see Figure 8). A child node with no patches will be deleted immediately. The ray tracing algorithm on a kd-tree runs in $log\ n$ time (where n is the number of primitives) and uses linear memory space.

This process is repeated down to the leaf nodes until a termination criterion is reached (e.g. a maximum tree depth, a minimum number of leaf patches or an automatic termination criteria (based on a heuristic cost function)).

The main benefit of the kd-tree structure compared to other space subdivision schemes is the improved adaptability to the geometry. The tree quality can be influenced significantly by the position of the splitting plane. Here a heuristic approach called surface area heuristic (SAH) has been established for the kd-tree splitting (Havran, 2000; Havran & Bittner, 2002). This method maximizes the empty space to construct an optimal kd-tree by minimizing a cost function (MacDonald & Booth, 1990). The cost function is based on the fact that the geometric probability of a ray intersecting any tree node $P(V'|V)$ is equal to the surface area of the node $SA(V')$ divided by the surface area of the upper node $SA(V)$:

$$P(V'|V) = \frac{SA(V')}{SA(V)}, \tag{24}$$

where V' is the child node of V and the corresponding surface area SA. The cost function

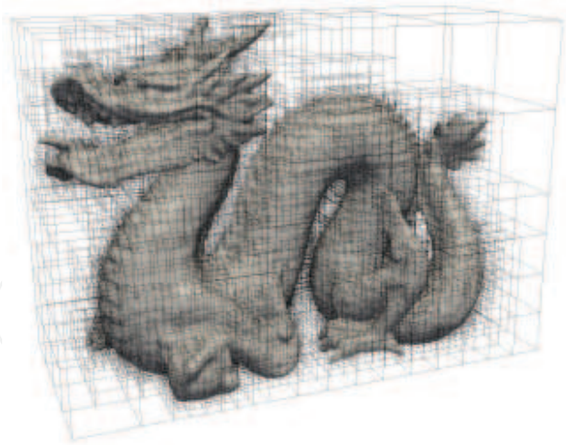

Fig. 9. Kd-tree example in 3D

is based on the following assumptions that the ray origins and directions are uniformly distributed, the cost of a traversal step C_t and a patch intersection C_i are known and the cost of intersecting n patches is directly proportional to the number of patches. Thus, the costs $C_N(V)$ for an inner tree node V can be calculated with the following equation:

$$\begin{aligned} C_N(V) &= C_t + n_l C_i P(V_l|V) + n_r C_i P(V_r|V) \\ &= C_t + C_i \left(n_l \frac{SA(V_l)}{SA(V)} + n_r \frac{SA(V_r)}{SA(V)} \right), \end{aligned} \tag{25}$$

where n_l is the number of patches overlapping the left node and analogously n_r is the number of patches overlapping the right node. In each recursive construction step, the cost function Eq. (25) can be evaluated for a certain number of possible split candidates. Here the best split position is coincident with the bounding box projection of the patch. So the cost function only needs to be evaluated at the triangle boundaries. With this approach the number of checked possible split candidates can be decreased dramatically. The best split position minimizes $C_N(V)$ Eq. (25). Fig.9 shows a three dimensional (3d) kd-tree example.
For the fast construction of heuristic optimized kd-trees a technique based on the sweeping algorithm has established, which works with a complexity of $O(n\ log^2\ n)$ (Szécsi, 2003; Pharr & Humphreys, 2004). This approach also includes an automatic termination criterion (ATC), based on the cost model, to decide whether to stop splitting or to continue subdividing a tree node (Havran & Bittner, 2002). An optimal kd-tree can thus be built without ad hoc defined constants.
The visibility detection between patches is processed by shooting rays on the kd-tree. As the traversal process starts at the root node, the child nodes are recursively tested for intersection with the ray until a leaf node is reached. All patches referenced from this leaf node are checked iteratively for intersection (fast ray-triangle and ray-box intersection tests can be found in e.g. (Badouel, 1990; Möller & Trumbore, 1997; Wald et al., 2001)). This approach allows to solve the visibility problem in $O(log\ n)$.

4. Preliminary applications

In this section some results of heat transfer and coupled heat transport simulations are shown. In the first application the energy distribution in porous asphalt induced by solar radiation is

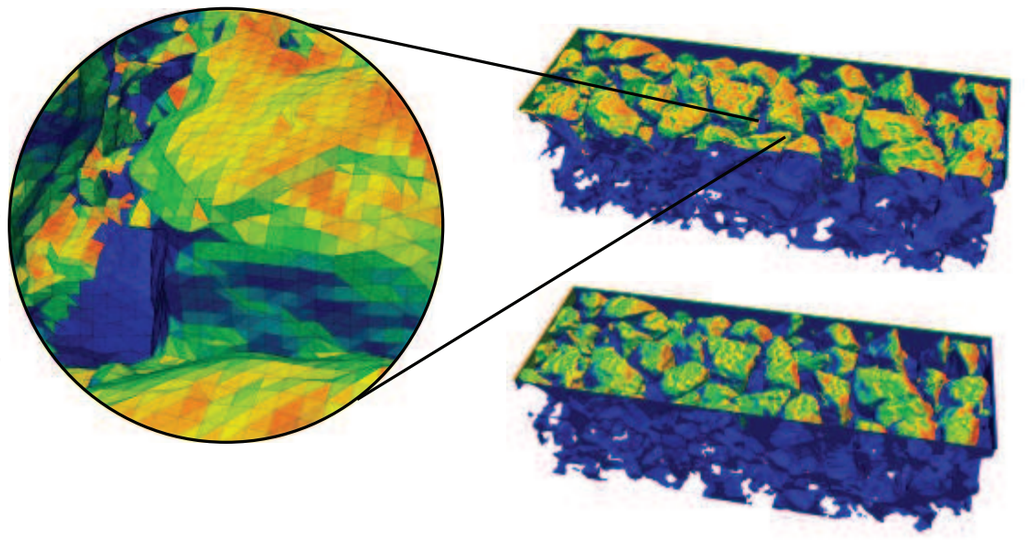

Fig. 10. Radiative energy distribution for different sun positions in a sample of porous asphalt with 50 million leaf triangles

simulated for different positions of the sun. Simulating the thermal behavior can help to optimize the composition and characteristics of asphalt. The geometric model is obtained by using a tomography scanner, which leads to complex models with very high resolutions (Ahrenholz, 2009). In this case a scan with 400x400x350 voxels is used, which is triangulated to a surface mesh (using e.g. the marching cubes method) with 10 million triangles. These high resolutions are necessary to represent the fine porous structure of the asphalt. The input surface mesh is adaptively refined during the hierarchical radiosity process to 50 million leaf triangles. Fig.10 shows the energy distribution over the surfaces for an equilibrium condition for two different sun position. The CPU time for this setup was about 700 seconds on an Intel Core2 Q9550 Quad-Cores, 8GB DDR2 Memory and Windows 7 64-bit.

A coupled variant is shown in Figure 11. Here, the surface temperatures are computed using the radiosity method introduced in section 3. These parameters are used as input values for the hTLBM simulation described in subsection 2.3. In this example the temperature distribution in a machine hall housing a server farm is simulated. This setup aims on the optimization of cooling and the identification of hot spots which can cause an overheating which potentially leads to malfunctioning server devices.

Another example demonstrating a combined simulation of radiation induced thermal energy and the resulting flow pattern also known as convection is shown in Figure 12. The aim of this simulation was to estimate the efficiency of three different versions of fassade constructions The simulation of the three different variants have been performed assuming worst case scenarios of the weather conditions (35° Celsius outside temperature, no wind). In order to obtain reasonable input data relative to the initial temperature distribution and the insertion of thermal energy into the system, the radiative heat transfer simulation section 3 has been performed in advance. Here, the surface temperature of all materials exposed to direct sunlight is determined and used as input data for LB simulations.

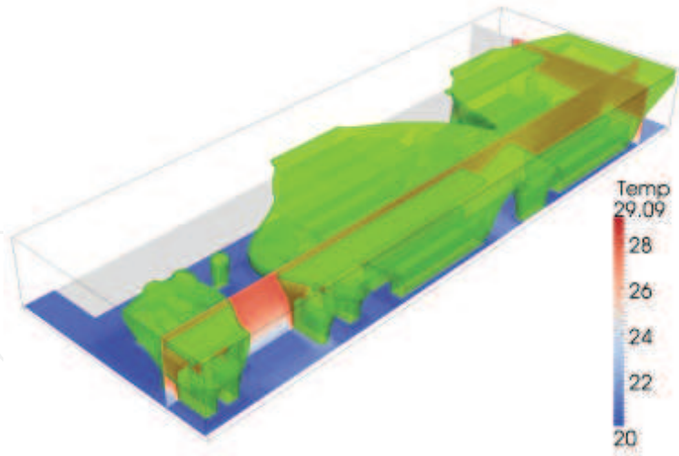

Fig. 11. Temperature distribution isosurfaces in a machine hall; the contours show the temperature boundary of 28° Celsius

5. Conclusion and outlook

With the radiosity-method the radiative heat transfer problem especially for applications in civil engineering can be efficiently and accurately simulated. Here, the hierarchical adaptive subdivision of the surfaces combined with a kd-tree based acceleration structure for the visibility detection dramatically decreases the runtime complexity of the radiation problem. Lattice Boltzmann fluid dynamics have been established as an alternative tool to solve different transport problems, including turbulent thermal flows. Its explicit numerical approach allows a straightforward coupling to other models representing structural dynamics or radiation and an efficient parallel implementation. The coupling between LBM and a radiation driven problem like convection has been succesfully demonstrated in the examples above.

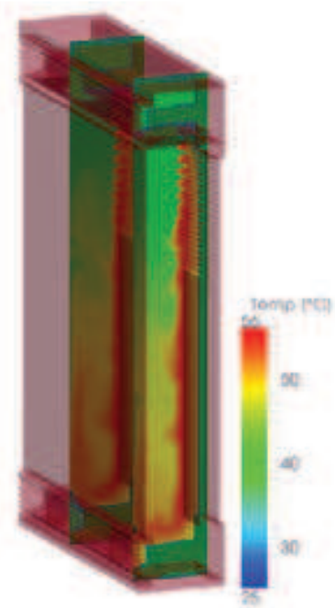

Fig. 12. Convection inside one floor of a buildings double fassade

Presently the bidirectional coupling of radiation induced heat and heat transport in fluid and solid is under investigation. Also the adaptation to special purpose hardware like GPUs is planed which is expected to deliver the accuracy of 3D transient transport simulations without the use of expensive supercomputers.

6. References

Ahrenholz, B. (2009). *Massively parallel simulations of multiphase- and multicomponent flows using lattice Boltzmann methods*, PhD thesis, Technischen Universität Carolo-Wilhelmina zu Braunschweig.

Alexander, F., Chen, S. & Sterling, J. (1993). Lattice Boltzmann thermohydrodynamics, *Physical Review E* 47: R2249.

Badouel, D. (1990). *An efficient ray-polygon intersection*, Academic Press Professional, Inc., San Diego, CA, USA.

Baehr, H. & Stephan, K. (2006). *Heat and Mass Transfer*, Springer Verlag.

Benzi, R., Succi, S. & Vergassola, M. (1992). The lattice Boltzmann equation: theory and applications, *Physics Reports* 222(3): 147–197.

Bhatnagar, P. L., Gross, E. P. & Krook, M. (1954). A Model for Collision Processes in Gases. I. Small Amplitude Processes in Charged and Neutral One-Component Systems, *Physical Review* 94: 511–525.

Bindick, S., Stiebler, M. & Krafczyk, M. (2010). Fast kd-tree based hierarchical radiosity for radiative heat transport problems, *submitted to: International Journal for Numerical Methods in Engineering* -: –.

Bohn, C.-A. & Garmann, R. (1995). A parallel approach to hierarchical radiosity, *University of West Bohemia*, pp. 26–35.

Cercignani, C., Illner, R. & Pulvirenti, M. (1994). *The Mathematical Theory of Dilute Gases*, Vol. 106 of *Applied Mathematical Sciences*, Springer Verlag, Berlin, Germany; New York, U.S.A.

Cercignani, C. & Penrose, R. (1998). *Ludwig Boltzmann: The Man Who Trusted Atoms*, Oxford University Press.

Chen, S. & Doolen, G. (1998). Lattice Boltzmann method for fluid flows, *Annual Review of Fluid Mechanics* 30: 329–364.

Cohen, M. F., Chen, S. E., Wallace, J. R. & Greenberg, D. P. (1988). A progressive refinement approach to fast radiosity image generation, *SIGGRAPH Comput. Graph.* 22(4): 75–84.

Cohen, M. F. & Greenberg, D. P. (1985). The hemi-cube: a radiosity solution for complex environments, *SIGGRAPH '85: Proceedings of the 12th annual conference on Computer graphics and interactive techniques*, ACM, New York, NY, USA, pp. 31–40.

d'Humières, D., Bouzidi, M. & Lallemand, P. (2001). Thirteen-velocity three-dimensional lattice boltzmann model, *Physical Review E* 63(6): 066702.

Dellar, P. (2003). Incompressible limits of lattice boltzmann equations using multiple relaxation times, *Journal of Computational Physics* 190: 351–370.

d'Humières, D. (1992). Generalized lattice-Boltzmann equations, *in* B. D. Shizgal & D. P. Weave (eds), *Rarefied Gas Dynamics: Theory and Simulations*, Vol. 159 of *Prog. Astronaut. Aeronaut.*, AIAA, Washington DC, pp. 450–458.

d'Humières, D., Ginzburg, I., Krafczyk, M., Lallemand, P. & Luo, L.-S. (2002). Multiple-relaxation-time lattice Boltzmann models in three dimensions, *Philosophical Transactions of the Royal Society A-Mathematical, Physical and Engineering Sciences* 360: 437–451.

Filippova, O. & Hänel, D. (2000). A novel lattice BGK approach for low Mach number combustion, *Journal of Computational Physics* 158: 139.

Frisch, U., d'Humières, D., Hasslacher, B., Lallemand, P., Pomeau, Y. & Rivet, J.-P. (1987). Lattice gas hydrodynamics in two and three dimensions, *Complex Systems* pp. 75–136.

Fujimoto, A., Tanaka, T. & Iwata, K. (1986). Arts: Accelerated ray-tracing system, *IEEE Comput. Graph. Appl.* 6(4): 16–26.

Geller, S., Krafczyk, M., Tölke, J., Turek, S. & Hron, J. (2006). Benchmark computations based on Lattice-Boltzmann, Finite Element and Finite Volume Methods for laminar Flows, *Computers & Fluids* 35: 888–897.

Ginzburg, I. & d'Humières, D. (1996). Local second-order boundary methods for lattice Boltzmann models, *Journal of Statistical Physics* 84: 927–971.

Glassner, A. S. (1984). Space subdivision for fast ray tracing, *IEEE Computer Graphics & Applications* 4(10): 15–22.

Goral, C. M., Torrance, K. E., Greenberg, D. P. & Battaile, B. (1984). Modeling the interaction of light between diffuse surfaces, *SIGGRAPH Comput. Graph.* 18(3): 213–222.

Hanrahan, P., Salzman, D. & Aupperle, L. (1991). A rapid hierarchical radiosity algorithm, *SIGGRAPH '91: Proceedings of the 18th annual conference on Computer graphics and interactive techniques*, ACM, New York, NY, USA, pp. 197–206.

Havran, V. (2000). *Heuristic Ray Shooting Algorithms*, Ph.d. thesis, Department of Computer Science and Engineering, Faculty of Electrical Engineering, Czech Technical University in Prague.

Havran, V. & Bittner, J. (2002). On Improving KD-Trees for Ray Shooting, *In Proc. of WSCG 2002 Conference*, pp. 209–217.

He, X. & Luo, L. S. (1997a). A priori derivation of the lattice boltzmann equation, *Physical Review E* 55(6): R6333–R6336.

He, X. & Luo, L.-S. (1997b). Theory of the lattice Boltzmann method: from the Boltzmann equation to the lattice Boltzmann equation, *Physical Review E* 56: 6811.

Higuera, F. J., Succi, S. & Benzi, R. (1989). Lattice Gas Dynamics with Enhanced Collisions, *Europhysics Letters* 9(4): 345–349.

Higuera, F. & Jiménez, J. (1989). Boltzmann approach to lattice gas simulations, *Europhysics Letters* 9: 663–668.

Hottel, H. C. & Cohen, E. S. (1958). Radiant heat exchange in a gas-filled enclosure: allowance for non-uniformity of gas temperature, *AIChE Journal* 4: 3–14.

Hou, S., Sterling, J., Chen, S. & Doolen, G. D. (1994). A Lattice Boltzmann Subgrid Model for High Reynolds Number Flows, *Contributions to Mineralogy and Petrology* pp. 1004–+.

Howell, J. R. (1982). *A Catalog of Radiation Configuration Factors*, McGraw-Hill, New York.

Junk, M., Klar, A. & Luo, L. (2005). Asymptotic analysis of the lattice Boltzmann equation, *jcp* 210: 676.

Krafczyk, M., Tölke, J. & Luo, L.-S. (2003). Large-Eddy Simulations with a Multiple-Relaxation-Time LBE Model, *APS Meeting Abstracts* pp. J7+.

Lallemand, P. & Luo, L.-S. (2000). Theory of the lattice Boltzmann method: Dispersion, dissipation, isotropy, Galilean invariance, and stability, *Physical Review E* 61: 6546–6562.

Lallemand, P. & Luo, L.-S. (2003). Theory of the lattice Boltzmann method: Acoustic and thermal properties in two and three dimensions, *Physical Review E* 68(3): 036706–+.

MacDonald, D. J. & Booth, K. S. (1990). Heuristics for ray tracing using space subdivision, *Vis. Comput.* 6(3): 153–166.

McNamara, G. & Zanetti, G. (1988). Use of the Boltzmann equation to simulate lattice-gas automata, *Physical Review Letters* 61: 2332–2335.

Modest, M. F. (2003). *Radiative Heat Transfer*, second edn, Academic Press, An imprint of Elsevier Science.

Möller, T. & Trumbore, B. (1997). Fast, Minimum Storage Ray-Triangle Intersection, *journal of graphics, gpu, and game tools* 2(1): 21–28.

Pellegrini, M. (1995). Monte carlo approximation of form factors with error bounded a priori, *SCG '95: Proceedings of the eleventh annual symposium on Computational geometry*, ACM, New York, NY, USA, pp. 287–296.

Pharr, M. & Humphreys, G. (2004). *Physically Based Rendering: From Theory to Implementation*, Morgan Kaufmann Publishers Inc., San Francisco, CA, USA.

Pianykh, O. S., Tyler, J. M. & Jr., W. N. W. (1998). Improved monte carlo form factor integration, *Computers & Graphics* 22(6): 723–734.

Podehl, A., Rauber, T. & Rünger, G. (1998). A shared-memory implementation of the hierarchical radiosity method, *Theor. Comput. Sci.* 196(1-2): 215–240.

Qian, Y. H. (1993). Simulating thermohydrodynamics with lattice BGK models, *Journal of Scientific Computing* 8: 231.

Qian, Y. H., d'Humières, D. & Lallemand, P. (1992). Lattice BGK models for Navier-Stokes equation, *Europhysics Letters* 17: 479–484.

Schäfer, S. (2000). *Efficient Object-Based Hierarchical Radiosity Methods*, PhD thesis, Technische Universität Braunschweig.

Shan, X. (1997). Simulation of Rayleigh-Bernard convection using the lattice Boltzmann method, *Physical Review E* 55: 2780.

Shaw, E. (1997). Hierarchical radiosity for dynamic environments, *Computer Graphics Forum* 16: 107–118.

Shevtsov, M., Soupikov, A. & Kapustin, A. (2007). Highly Parallel Fast KD-tree Construction for Interactive Ray Tracing of Dynamic Scenes, *Comput. Graph. Forum* 26(3): 395–404.

Siegel, R. & Howell, J. R. (2002). *Thermal radiation heat transfer*, third edn, Taylor & Francis Inc.

Sinop, A. K., Abaci, T., Akkuş, U., Gürsoy, A. & Güdükbay, U. (2005). Phr: A parallel hierarchical radiosity system with dynamic load balancing, *J. Supercomput.* 31(3): 249–263.

Sterling, J. D. & Chen, S. (1996). Stability analysis of lattice Boltzmann methods, *Journal of Computational Physics* 123(1): 196–206.

Succi, S. (2001). *The Lattice Boltzmann Equation for Fluid Dynamics and Beyond*, Oxford University Press, Oxford.

Szécsi, L. (2003). *Graphics programming methods*, Charles River Media, Inc., Rockland, MA, USA, chapter An effective implementation of the k-D tree, pp. 315–326.

Szirmay-Kalos, L., Havran, V., Balázs, B. & Szécsi, L. (2002). On the Efficiency of Ray-shooting Acceleration Schemes, *in* A. Chalmers (ed.), *Proceedings of the 18th Spring Conference on Computer Graphics (SCCG 2002)*, ACM Siggraph, Budmerice, Slovakia, pp. 89–98.

Tampieri, F. (1992). *Accurate form-factor computation*, Academic Press Professional, Inc., San Diego, CA, USA.

Tlke, J. (2006). A thermal model based on the lattice boltzmann method for low mach number compressible flows, *Journal of Computational and Theoretical Nanoscience* 3(4): 579–587.

Tlke, J. & Krafczyk, M. (2008). Teraflop computing on a desktop pc with gpus for 3d cfd, *International Journal of Computational Fluid Dynamics* 22(7): 443–456.
URL: *http://dx.doi.org/10.1080/10618560802238275*

Vahala, L., Wah, D., Vahala, G., Carter, J. & Pavlo, P. (2000). Thermal Lattice Boltzmann Simulation for Multispecies Fluid Equilibration, *Physical Review E* 62: 507.

van Treeck, C., Rank, E., Krafczyk, M., Tölke, J. & Nachtwey, B. (2006). Extension of a hybrid thermal LBE scheme for Large-Eddy simulations of turbulent convective flows, *Computers & Fluids* 35(8–9): 863–871.

Wald, I., Slusallek, P., Benthin, C. & Wagner, M. (2001). Interactive Rendering with Coherent Ray Tracing, *Computer Graphics Forum*, pp. 153–164.

Wallace, J. R., Elmquist, K. A. & Haines, E. A. (1989). A ray tracing algorithm for progressive radiosity, *SIGGRAPH Comput. Graph.* 23(3): 315–324.

Welty, J. R., Wicks, C. E., Wilson, R. E. & Rorrer, G. (2001). *Fundamentals of Momentum, Heat and Mass Transfer*, John Wiley & Sons, Inc.

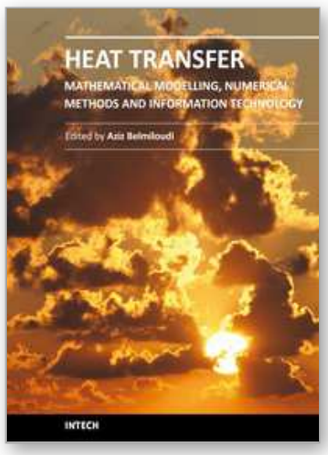

Heat Transfer - Mathematical Modelling, Numerical Methods and Information Technology

Edited by Prof. Aziz Belmiloudi

ISBN 978-953-307-550-1
Hard cover, 642 pages
Publisher InTech
Published online 14, February, 2011
Published in print edition February, 2011

Over the past few decades there has been a prolific increase in research and development in area of heat transfer, heat exchangers and their associated technologies. This book is a collection of current research in the above mentioned areas and describes modelling, numerical methods, simulation and information technology with modern ideas and methods to analyse and enhance heat transfer for single and multiphase systems. The topics considered include various basic concepts of heat transfer, the fundamental modes of heat transfer (namely conduction, convection and radiation), thermophysical properties, computational methodologies, control, stabilization and optimization problems, condensation, boiling and freezing, with many real-world problems and important modern applications. The book is divided in four sections : "Inverse, Stabilization and Optimization Problems", "Numerical Methods and Calculations", "Heat Transfer in Mini/Micro Systems", "Energy Transfer and Solid Materials", and each section discusses various issues, methods and applications in accordance with the subjects. The combination of fundamental approach with many important practical applications of current interest will make this book of interest to researchers, scientists, engineers and graduate students in many disciplines, who make use of mathematical modelling, inverse problems, implementation of recently developed numerical methods in this multidisciplinary field as well as to experimental and theoretical researchers in the field of heat and mass transfer.

INTECH
open science | open minds

InTech Europe
University Campus STeP Ri
Slavka Krautzeka 83/A
51000 Rijeka, Croatia
Phone: +385 (51) 770 447

InTech China
Unit 405, Office Block, Hotel Equatorial Shanghai
No.65, Yan An Road (West), Shanghai, 200040, China
中国上海市延安西路65号上海国际贵都大饭店办公楼405单元
Phone: +86-21-62489820

Fax: +385 (51) 686 166
www.intechopen.com

Fax: +86-21-62489821

IntechOpen